Numerical Simulations of the Scattered Field Near a Statistically Rough Air-Ground Interface

Alexander G. Yarovoy, *Member, IEEE*, Christos N. Vazouras, John G. Fikioris, and Leo P. Ligthart, *Fellow, IEEE*

***Abstract*—The two-dimensional problem of horizontally polarized wave scattering from an air-ground interface is considered. The diffraction problem is formulated by means of the extinction theorem, leading to a system of two simultaneous surface integral equations. The small-slope approximation has been used to solve this system. This solution was used as a fast forward solver in the Monte Carlo simulations of the scattered field near to the rough interface. Properties of the reflected field have been investigated for a single realization of the rough interface as well as for a statistical ensemble of such interfaces. Special attention has been paid to the phase of the reflected field (in the case of a single realization) and to the variance of the reflected field (in the case of a statistical ensemble), which has direct relation with the surface clutter in ground penetrating radars. A principal possibility to retrieve a surface profile from interferometric measurements of the reflected field near the surface is demonstrated.**

***Index Terms*—Ground penetrating radar, rough surface scattering, surface clutter.**

I. Introduction

In ground penetrating radar (GPR) systems, which operate close to the air-ground interface, scattering from the rough interface plays an important role [1], [2]. This scattered field is measured by GPR as clutter, which masks the response from buried targets and reduces the available dynamic range of GPR. In numerous previous studies of wave scattering from rough surfaces, far-field characteristics of the scattered field have been investigated (see e.g., classical books [3], [4]). Much less attention has been paid to the scattered field near the rough surface (see, e.g., [5]). The main reason for this is that it is difficult to derive any analytical approximation for the field. With the development of direct numerical methods for the scattered field computation, this problem can be overcome. In this paper, we investigate fluctuations of the scattered field near a rough interface between two dielectric media using a numerical technique based on the Monte Carlo approach.

Manuscript received August 20, 2001; revised December 10, 2002. This work was supported in part by the Dutch Technology Foundation STW, the Applied Science Division of NWO, and in part by the Technology Program of the Ministry of Economic Affairs of The Netherlands.

A. G. Yarovoy and L. P. Ligthart are with the International Research Centre for Telecommunications-Transmission and Radar, Delft University of Technology, Delft, 2628 CD Delft, The Netherlands (e-mail: a.yarovoy@irctr.tudelft.nl; l.p.ligthart@irctr.tudelft.nl).

C. N. Vazouras was with the National Technical University of Athens, Athens, 15773, Greece. He is now with the Hellenic Naval Academy, Piraeus 18539, Greece (e-mail: chvaz@gsrt.gr).

J. G. Fikioris is with the Department of Electrical and Computer Engineering, National Technical University of Athens, Athens 15773, Greece (e-mail: ifikio@central.ntua.gr).

Digital Object Identifier 10.1109/TAP.2004.825499

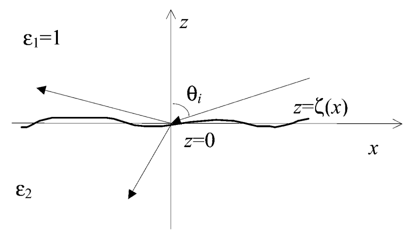

Fig. 1. Geometry of the problem.

For the Monte Carlo simulations a fast solver for the forward scattering problem is needed. Direct numerical simulation based on integral equation methods requires considerable computational resources (for more details, see, e.g., [6]). If one takes into account that the surface roughness has a typical height below 10 cm, that the surface slope is not very steep and that the GPR systems typically use frequencies below 1 GHz [1], one can see that it is possible to use a relatively simple perturbative approach like the small-slope approximation [7] or similar techniques [8]–[10] to solve the forward scattering problem. Such an approach can speed up Monte Carlo simulations tremendously in comparison with a direct numerical solution based on the integral equation methods.

II. Formulation of the Problem

We consider two homogeneous half spaces, characterized by the dielectric permittivities ε_1 and ε_2, respectively, while the magnetic permeability of the whole space equals the one for free space (μ_0). The upper half space is supposed to be air, thus ε_1 equals the free-space value ε_0, and the lower half space contains a lossy dielectric medium (ground), so ε_2 can be presented as $\varepsilon_2 \equiv \varepsilon_{2r}\varepsilon_0 + i\sigma_2/\omega$, where ε_{2r} is the real part of the ground dielectric permittivity, σ_2 is the ground conductivity, and the circular frequency ω corresponds to an $\exp(-j\omega t)$ time dependence. The propagation constants in both half spaces are $k_1 = k_0 \equiv \omega\sqrt{\varepsilon_0\mu_0}$ and $k_2 = \omega\sqrt{\varepsilon_2\mu_0}$, respectively.

We limit our consideration to the two-dimensional (2-D) case, where the interface between half spaces is described by a profile function $z = \zeta(x)$ (see Fig. 1). We consider the case of horizontal (or TE-) polarization and the letter Ψ denotes the y-component of the electric field. The TM case can be treated similarly. Physically the 2-D case means that the characteristic size of surface inhomogeneities in one direction is considerably larger than that in the perpendicular direction and larger than the wavelength of the incident field. Practically it means also that this characteristic size is larger than the size of an antenna spot on the interface.

We formulate the scattering problem based on the extinction theorem [or the extended boundary condition (EBC) or the null-field method] [11], [12]. By application of Green's identity and Helmholtz equation, the following integral equations can be derived

$$\Psi_{\mathrm{inc}}(\vec{r}) + \int_s \Big\{ \Psi^+(\vec{r}')\,[\hat{n}\cdot\nabla' G_0(\vec{r}-\vec{r}')] - \left[\hat{n}\cdot\nabla'\Psi^+(\vec{r}')\right] G_0(\vec{r}-\vec{r}') \Big\} dS' = \begin{cases} \Psi(\vec{r}), z > \zeta(x') & \text{(1a)} \\ 0, z < \zeta(x') & \text{(1b)} \end{cases}$$

$$\int_s \Big\{ \left[\hat{n}\cdot\nabla'\Psi^-(\vec{r}')\right] G_2(\vec{r}-\vec{r}') - \Psi^-(\vec{r}') \cdot [\hat{n}\cdot\nabla' G_2(\vec{r}-\vec{r}')] \Big\} dS' = \begin{cases} 0, z > \zeta(x') & \text{(2a)} \\ \Psi(\vec{r}), z < \zeta(x') & \text{(2b)} \end{cases}$$

where G_0 and G_2 are the 2-D Green functions corresponding to homogeneous spaces with propagation constant k_0 and k_2, respectively. In (1) and (2), primed variables denote points on the surface, i.e., $z' = \zeta(x')$, the integration is over the whole surface, and the superscript "+" or "−" denotes the total electric field value on the upper or lower side of the rough surface, respectively. The vector $\hat{n}$ is unitary, normal to the surface and directed upwards, corresponding to

$$\vec{n} = \frac{\vec{z} - \frac{d\zeta(x')}{dx'}\vec{x}}{\sqrt{1 + \left(\frac{d\zeta(x')}{dx'}\right)^2}} \tag{3}$$

and $\vec{n}\cdot\nabla'$ is the normal derivative with respect to the primed argument. As is well known, in the EBC approach the observation point is placed in an appropriate subset of each half space, rather than on the rough interface itself, and thus the singularity exhibited by the Green function when the observation point traverses the source point is avoided.

Using the boundary conditions on the rough surface resulting from continuity of the tangential component of the electric field and of the normal component of the electric flux vector

$$\Psi^+(\vec{r}') = \Psi^-(\vec{r}'), \quad \vec{n}\cdot\nabla'\Psi^+(\vec{r}') = \vec{n}\cdot\nabla'\Psi^-(\vec{r}') \tag{4}$$

we derive from (1b) and (2a) the pair of simultaneous integral equations for the unknown functions Ψ^+ and $\vec{n}\cdot\nabla'\Psi^+$, while (1a) and (2a) are essentially an expression of the well-known Helmholtz–Kirchhoff integral formula and they may subsequently be used to calculate the scattered fields. We introduce the following notation for the unknown source functions

$$\begin{aligned} f(x') &= j\vec{n}\cdot\nabla'\Psi^+(\vec{r}')\sqrt{1 + \left[\frac{d\zeta(x')}{dx'}\right]^2} \\ g(x') &= \Psi^+(\vec{r}') \end{aligned} \tag{5}$$

substitute the well-known explicit integral expressions for G_0 and G_2 into (1) and (2), assume that the incident field is a plane wave

$$\Psi_{\mathrm{inc}}(\vec{r}) = \exp[jk_0(x\sin\theta_i - z\cos\theta_i)] \tag{6}$$

which impinges from the upper half-space with the incidence angle θ_i (measured from the z axis). Finally, we carry out the differentiations and interchange the order of integration (an operation that should be interpreted in the sense of generalized functions) in (1) and (2). As a result we arrive at the following system of simultaneous integral, or, more properly speaking, operator equations

$$\int_{-\infty}^{+\infty} \exp[-j\kappa x + j\gamma_0(\kappa)\zeta(x)] \cdot \left\{ f(x) + \left[\gamma_0(\kappa) + \kappa\frac{d\zeta(x)}{dx}\right] g(x) \right\} dx = 4\pi\gamma_0(\kappa_0\delta(\kappa-\kappa_0)) \tag{7a}$$

$$\int_{-\infty}^{+\infty} \exp[-j\kappa x - j\gamma_2(\kappa)\zeta(x)] \cdot \left\{ f(x) + \left[\kappa\frac{d\zeta(x)}{dx} - \gamma_2(\kappa)\right] g(x) \right\} dx = 0 \tag{7b}$$

where

$$\gamma_i(\kappa) = \left(k_i^2 - \kappa^2\right)^{1/2}, \quad i = 0, 2 \tag{8}$$

$$\kappa_0 = k_0 \sin\theta_i, \quad \gamma_0(\kappa_0) = k_0\cos\theta_i. \tag{9}$$

The square root is defined according to the radiation conditions, so that $\mathrm{Re}[\gamma_i(\kappa)] \geq 0, \mathrm{Im}[\gamma_i(\kappa)] \geq 0$. The reflected field, derived from (1a) in a similar manner, is given by

$$\Psi_r(\vec{r}) = \Psi(\vec{r}) - \Psi_{\mathrm{inc}}(\vec{r}) = \int_{-\infty}^{+\infty} A^{(r)}(\kappa)\exp[j\kappa x + j\gamma_0(\kappa)z]d\kappa \quad z > \max_x\{\zeta(X)\} \tag{10a}$$

and the transmitted field inside the ground, from (2b), as

$$\Psi_t(\vec{r}) = \Psi(\vec{r}) = \int_{-\infty}^{+\infty} A^{(t)}(\kappa)\exp[j\kappa x - j\gamma_2(\kappa)z]d\kappa \quad z < \min_x\{\zeta(x)\} \tag{10b}$$

where

$$A^{(r)}(\kappa) = -\frac{1}{4\pi\gamma_0(\kappa)}\int_{-\infty}^{+\infty} \exp\left[-j\kappa x' - j\gamma_0(\kappa)\zeta(x')\right] \cdot \left\{ f(x') + g(x')\left[\kappa\frac{d\zeta(x')}{dx'} - \gamma_0(\kappa)\right]\right\} dx' \tag{11a}$$

$$A^{(t)}(\kappa) = \frac{1}{4\pi\gamma_2(\kappa)}\int_{-\infty}^{+\infty} \exp\left[-j\kappa x' + j\gamma_2(\kappa)\zeta(x')\right] \cdot \left\{ f(x') + g(x')\left[\kappa\frac{d\zeta(x')}{dx'} + \gamma_2(\kappa)\right]\right\} dx'. \tag{11b}$$

From now on, the limits of integration $-\infty$ to $+\infty$ will be omitted for simplicity.

At very low (near-grazing) scattering angles when $\kappa \to \pm k_0$ and $\gamma_0(\kappa) \to 0$ the singularity appears in (11a). It has been found that this singularity causes a loss of accuracy in the near-grazing portion of the reflected angular spectrum. Scattered waves at near-grazing directions have little effect on the total scattered power, but they may be important for the field values just above the rough surface, which are of interest in this study. To avoid the singularity we use a linear combination of (11a) and (7a), which yields

$$A^{(r)}(\kappa) = -\delta(\kappa-\kappa_0) + \frac{1}{2\pi}\int_{-\infty}^{+\infty} \exp\left[-j\kappa x\right] \cdot \left\{ j\left[f(x) + \kappa \frac{d\zeta(x)}{dx} g(x)\right] \frac{\sin\left[\gamma_0(\kappa)\zeta(x)\right]}{\gamma_0(\kappa)} + g(x)\cos\left[\gamma_0(\kappa)\zeta(x)\right]\right\} dx. \tag{12}$$

Equation (12) differs from (11a) only for any approximate solution of (7). If exact solutions f and g of the system (7) were available, (12) would be equivalent to (11a). A similar singularity can occur for the transmitted field in (11b) (though only in the case of lossless ground). Then this problem may be treated in a similar manner.

III. Iterative Solution

In the case of an interface of an arbitrary profile $\zeta(x)$, the system (7) cannot be solved analytically. The implementation of different numerical methods is still limited by the amount of required CPU time and computer memory. We apply to this system the small-slope approximation [13]–[16] in a similar manner as in [10]. We represent both unknown functions in the form

$$f(x) = \exp[-j\gamma_0(\kappa_0)\zeta(x)] \sum_{m=0}^{+\infty} f_m(x)$$
$$g(x) = \exp[-j\gamma_0(\kappa_0)\zeta(x)] \sum_{m=0}^{+\infty} g_m(x) \tag{13}$$

where $f_m(x)$, $g_m(x)$ are functions of order $\zeta^m(x)$. We do not discuss the convergence of (14) here, assuming that it holds in some appropriate sense. Using the procedure described in [10], one can derive a pair of iterative relations for f_m and g_m

$$\begin{aligned}\tilde{f}_m(\kappa) = &-\frac{1}{2\pi}\frac{1}{\gamma_0(\kappa)+\gamma_2(\kappa)}\sum_{n=0}^{m-1}\frac{j^{m-n}}{(m-n)!} \\ &\cdot\left\{\left[\gamma_2(\kappa)q^{m-n}(\kappa)+\gamma_0(\kappa)(-1)^{m-n}p^{m-n}(\kappa)\right]\right. \\ &\cdot\int Z_{m-n}(\kappa-\kappa')\tilde{f}_n(\kappa')d\kappa' \\ &+\gamma_0(\kappa)\gamma_2(\kappa)\left[q^{m-n}(\kappa)-(-1)^{m-n}p^{m-n}(\kappa)\right] \\ &\cdot\int Z_{m-n}(\kappa-\kappa')\tilde{g}_n(\kappa')d\kappa' \\ &+\kappa\left[\gamma_2(\kappa)q^{m-n-1}(\kappa)\right. \\ &\left.+\gamma_0(\kappa)(-1)^{m-n-1}p^{m-n-1}(\kappa)\right] \\ &\left.\cdot\int(\kappa-\kappa')Z_{m-n}(\kappa-\kappa')\tilde{g}_n(\kappa')d\kappa'\right\}\end{aligned}$$

$$\begin{aligned}\tilde{g}_m(\kappa) = &-\frac{1}{2\pi}\frac{1}{\gamma_0(\kappa)+\gamma_2(\kappa)}\sum_{n=0}^{m-1}\frac{j^{m-n}}{(m-n)!} \\ &\cdot\left\{\left[q^{m-n}(\kappa)-(-1)^{m-n}p^{m-n}(\kappa)\right]\right. \\ &\cdot\int Z_{m-n}(\kappa-\kappa')\tilde{f}_n(\kappa')d\kappa' \\ &+\left[\gamma_0(\kappa)q^{m-n}(\kappa)+\gamma_2(\kappa)(-1)^{m-n}p^{m-n}(\kappa)\right] \\ &\cdot\int Z_{m-n}(\kappa-\kappa')\tilde{g}_n(\kappa')d\kappa'+ \\ &+\kappa\left[q^{m-n-1}(\kappa)-(-1)^{m-n-1}p^{m-n-1}(\kappa)\right] \\ &\left.\cdot\int(\kappa-\kappa')Z_{m-n}(\kappa-\kappa')\tilde{g}_n(\kappa')d\kappa'\right\}.\end{aligned} \tag{14}$$

Here we used the notations

$$Z_m(\kappa) \equiv \int \exp\left[-j\kappa x\right]\zeta^m(x)\,dx$$
$$q(\kappa) = \gamma_0(\kappa) - \gamma_0(\kappa_0), \quad p(\kappa) = \gamma_2(\kappa) + \gamma_0(\kappa_0).$$

In (14), as well as throughout the following, the tilde ($\sim$) denotes the Fourier transform, i.e.

$$\tilde{f}(\kappa) \equiv \Im\{f(x)\} \equiv \int \exp(-j\kappa x) f(x) dx.$$

For the selected power spectrum of the surface roughness (see next section) and the surface root-mean-square (rms) height $\sigma_h = 0.1\lambda_0$, $\lambda_0 \equiv 2\pi k_0^{-1}$ (which results in a surface rms slope of about 0.14 radians), the perturbative solution (13) and (14) is roughly 500 times faster than the method of moment solution developed in [10].

IV. Monte Carlo Simulation

To examine the statistical properties of the reflected field we use the Monte Carlo approach, which employs three major steps: generation of an ensemble of surface profiles with the desired probability distribution and power spectrum; calculation of the reflected field for each realization of the surface; and calculation of statistical moments of the reflected field by numerical averaging over the whole ensemble. To generate an ensemble of statistically rough surfaces with predefined statistical properties we used the algorithm described in [17] and [18]. The generated surface patch of final length is duplicated in the space domain to construct infinite periodical surface. Periodicity of the surface allows us to use discrete Fourier transform to evaluate numerically integrals from (11) and (12). On the other hand, periodicity of the surface causes edge effects [19] (some distortion of statistical properties of the scattered field, which are often referred to as spectral leakage) and discretization (quantization) of the wavenumber spectrum. The former phenomenon might play an important role for the scattered field in the far-zone of the surface patch and tapering of the incident wave is typically introduced in an attempt to minimize it [19]. However, in the near field the edge effects will show up mainly locally nearby to the ends of the surface patch and it is sufficient to use sufficiently large patch to decrease impact of these edge effects. Another opportunity is windowing of the data (e.g., as it has been used in [19]) to obtain a reliable statistical estimates. The latter phenomenon (discretization of the wavenumber spectrum) requires a proper choice of the surface patch length (a discretization step in the wavenumber domain should be much smaller than a characteristic width of the surface power spectrum) and causes discretization of the incident angle $\theta_{\rm inc}$.

The main difference of our approach from previous studies is utilization in the Monte Carlo simulations of a band-limited power-law spectrum as suggested, e.g., in [20]

$$W(\kappa) = \begin{cases} \dfrac{2\pi(s-1)\kappa_l^{s-1}\kappa^{-s}}{1-\left(\dfrac{\kappa_l}{\kappa_u}\right)^{s-1}}, & \kappa_1 \leq \kappa \leq \kappa_u \\ 0, & \text{elsewhere} \end{cases} \tag{15}$$

where the exponent s is usually between 3 and 4, and κ_l and κ_u are the lower and upper cutoff wavenumbers, respectively. The choice of the power-law spectrum is motivated by recent studies [20], [21] which show that the spectrum (15) is much more suitable for the description of natural surfaces than the Gaussian spectrum.

Use of the spectrum (15) requires a careful choice of the upper bound for the value of κ_u. At the first glance, κ_u is restricted by the sampling theorem

$$\kappa_u \leq \frac{\pi}{d}$$

where d is the sampling period. However, the use of higher-order terms in the perturbation series imposes more stringent limitations. The nth term of the perturbation series contains the nth power of the profile function $\zeta(x)$ (in the space domain). Thus, the spectral bandwidth of this term extends to n times the bandwidth κ_u of the profile function. Taking into account the shift in the spectral domain on the wavenumber $\kappa_0 = k_0 \sin\theta_i$ of the incident field, we arrive at the following estimation of the spectral bandwidth:

$$n_{\max}\kappa_u + |k_0 \sin\theta_i| \leq n_{\max}\kappa_u + k_0$$

where $n_{\max}$ is the highest order of the perturbation series terms kept in the approximate expressions for the unknown functions f and g. The spectral bandwidth of all perturbation terms should not exceed the limitation imposed by the sampling theorem

$$\kappa_{\max} = \frac{\pi}{d}.$$

Thus, in the most general case, the upper bound for the bandwidth of the profile function is

$$\kappa_u \leq \frac{\pi}{n_{\max} d} - \frac{k_0}{n_{\max}}. \tag{16}$$

Numerical tests have shown that failure to comply with this restriction results in high-frequency oscillations in the values computed for the surface unknown functions. The high-frequency character of these oscillations is attributed to the fact that violation of (16) distorts the upper side of the spectrum of the corresponding perturbation terms.

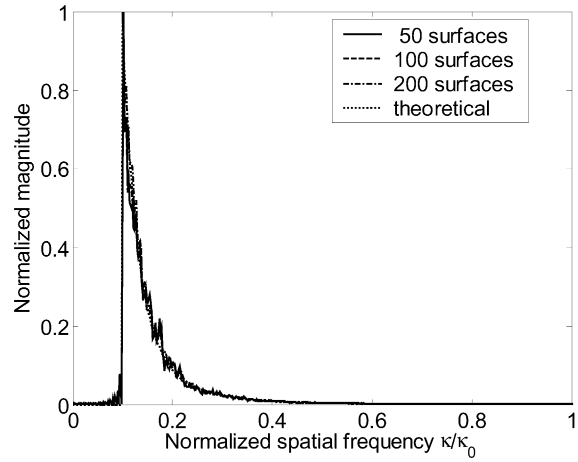

Fig. 2. Surface power spectrum $s = 3.5, = 0.04\lambda_0$ ($s = 3.5, \kappa_l = 0.1k_0, \kappa_u = 2k_0$).

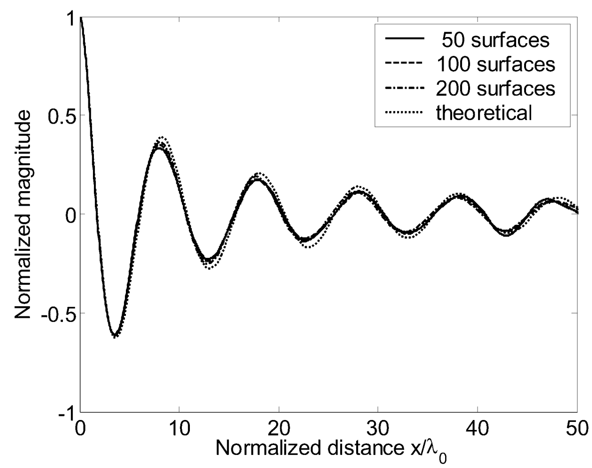

Fig. 3. Surface correlation function $s = 3.5, \kappa_l = 0.1k_0, \kappa_u = 2k_0$.

Regarding to the lower cutoff wavenumber κ_l, it should be chosen at least several times large than the discretization step in the wavenumber domain in order to obtain a proper surface power spectrum estimate.

Because we had changed the surface power spectrum compared to that in previous studies [17], [18], it was necessary to check again whether there is convergence of the power spectrum (and the correlation function) of the generated surface ensemble to the predetermined surface power spectrum (and the correlation function) during Monte Carlo simulation. It has been found that the desired shape of the surface power spectrum is achieved after averaging of 50 realizations of the surface (with 4096 sampling points). Further increase of the number of averaging suppresses the small ripples from the low-frequency part of the spectrum, but this does not change the shape of the spectral estimates (see Fig. 2). The estimates of surface correlation function change only slightly when the averaging number is increased to above 50 (Fig. 3). The impact of the lower cutoff wavenumber κ_l on the surface correlation function is shown in Fig. 4. By a fixed rms height of the surface decrease of the lower cutoff wavenumber causes “stretching” of the surface correlation function, so the inversed lower cutoff wavenumber $1/\kappa_l$ plays a role of the spatial correlation length.

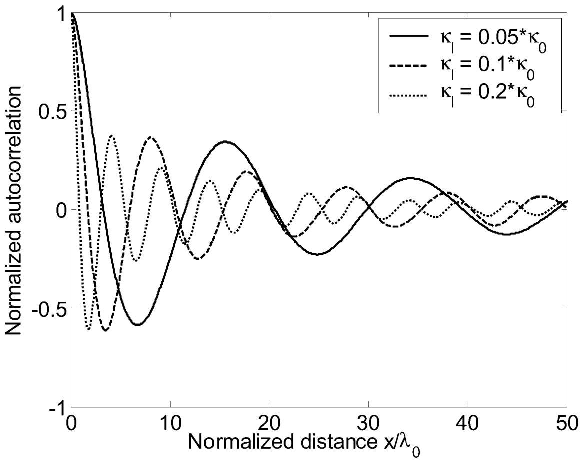

Fig. 4. Surface correlation function (calculated from 200 realizations of the surface profile) for different values of κ_l ($s = 3.5, \kappa_u = 2k_0, \sigma_h = 0.1\lambda_0$)).

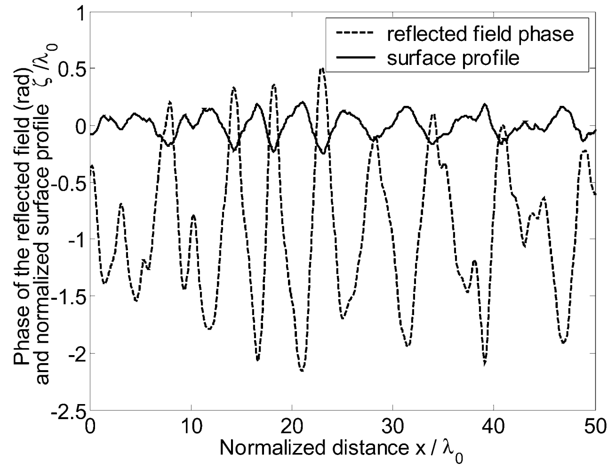

Fig. 5. Phase of the reflected field versus distance along the patch. The surface rms height σ_h equals $0.33\lambda_0$, the elevation of the observation point above the mean position of the rough surface equals $0.33\lambda_0$, the dielectric permittivity of the ground ε_{2r} equals 6, and the ground conductivity σ_2 equals 0.01 S/m.

At the final stage of the Monte Carlo procedure, the calculated reflected electric field is averaged over all realizations of the surface to obtain $\langle E_r(x_n)\rangle$, where angle brackets $\langle\ldots\rangle$ mean ensemble averaging. The field $\langle E_r(x_n)\rangle$ can be further averaged in the space domain, i.e., over the number of samples representing the surface patch

$$E_{\mathrm{r,mean}} = \frac{1}{N}\sum_{n=1}^{N}\langle E_r(x_n)\rangle \tag{17}$$

providing an estimation of the coherent component of the reflected field. Fluctuations of the reflected field are estimated by their variance σ_e, where

$$\sigma_e^2 \equiv \left\langle (E_r - \langle E_r\rangle)(E_r - \langle E_r\rangle)^*\right\rangle \tag{18}$$

and by the correlation function.

V. Numerical Results and Discussion

The simulations have been carried out for the following parameter values. The frequency of the incident wave is chosen as 100 MHz (which determines typical values of dielectric permittivity and ohmic losses of the ground) and the incidence angle is chosen equal to zero ($\theta_{\mathrm{inc}} = 0^\circ$). The power s in the surface power spectrum has been selected based on studies of natural surfaces [20], [21]. Aiming to implement a really wide-band spectrum we chose κ_l considerably lower than the wavenumber of the incident field and κ_u higher than the wavenumber of the incident field. This result in the following parameters of the power-law spectrum

$$s = 3.5, \quad \kappa_l = 0.1k_0, \quad \kappa_u = 2k_0.$$

In a few cases we have used other than $0.1k_0$ values for the lower cutoff wavenumber, and in these cases the value of κ_l will be mentioned explicitly. Having in mind (16) we chose a sampling interval (discretization step) of $d = 0.05\lambda_0$, which corresponds to 20 sampling points per the wavelength (in previous studies [17]–[19] for surfaces with Gaussian surface power spectrum a number of sampling points per the wavelength of the incident field have chosen from 5 to 10 been used, while the band-limited power-law spectrum requires in general denser sampling due to its larger bandwidth in wavenumber domain). To achieve considerably denser wavenumber spectrum and to minimize edge effects we chose the total length of the simulated surface patch of $N = 4096$ samples. To check the influence of the patch length on the statistical estimates for the reflected field we performed also simulations for the shorter patch (with $N = 1024$ samples). The differences less than 1% have been observed in the statistical estimates for these two patches. From that experiment we have concluded that the surface patch with $N = 4096$ samples is long enough to provide sufficiently accurate results.

The accuracy of the simulations has been checked thoroughly. For a single realization of the random surface from each ensemble, a comparison with the method of moments [10] results has been made. The accuracy of the simulation has been estimated based on the relative error, which is defined as the normalized rms difference between the reflected field as found by the perturbation technique and the MoM solution

$$\Sigma = \left(\frac{\sum_n \left|E_r(x_n) - E_r^M(x_n)\right|^2}{\sum_n \left|E_r^M(x_n)\right|^2}\right)^{1/2} \tag{19}$$

where the superscript M denotes the corresponding values found by the benchmark. A threshold value of 1% for the relative error Σ has been chosen, so that the results obtained by the perturbative technique can be considered as "exact" ones. To achieve this threshold, terms up to the fifth-order have been used in the perturbative solution.

We start our numerical analysis with a description of the scattering from a single realization of the air-ground interface. In this analysis, we selected values of the surface rms height σ_h in the range $\sigma_h \leq 0.1\lambda_0$, because for a chosen power spectrum of the surface roughness the surface rms height of $\sigma_h = 0.1\lambda_0$ results in a surface rms slope of about 0.14 radians. Such value of the slope is very close to the limit, after which the power series (14) do not converge any more. We found that for all selected values of the surface rms height σ_h, the phase of the reflected field near the surface follows the surface profile (Fig. 5). The

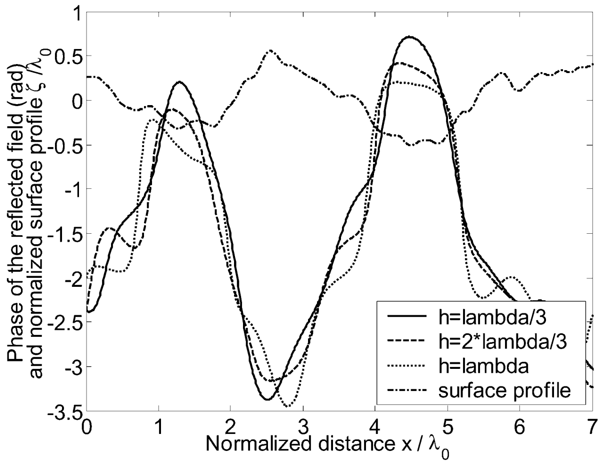

Fig. 6. Phase of the reflected field versus distance along the patch for different elevations of the observation point. The surface rms height σ_h equals $0.1\lambda_0$, the dielectric permittivity of the ground ε_{2r} equals 6, and the ground conductivity σ_2 equals 0.01 S/m.

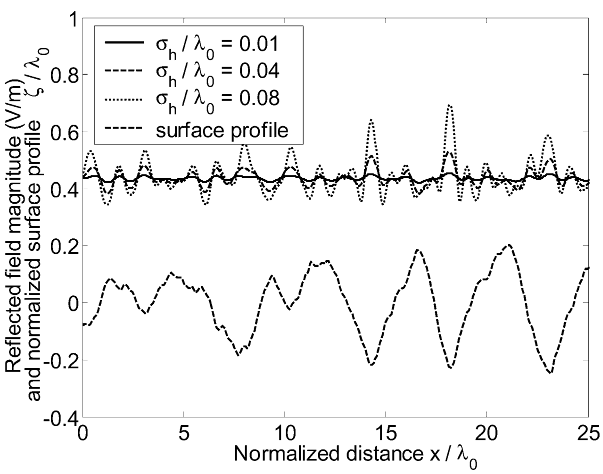

Fig. 7. Magnitude of the reflected field versus distance over the patch for different values of the surface rms height. The elevation of the observation point above the mean position of the rough surface equals $0.33\lambda_0$. The dielectric permittivity of the ground ε_{2r} equals 6, and the ground conductivity σ_2 equals 0.01 S/m. The surface profile is shown for the case $\sigma_h = 0.04\lambda_0$.

correlation coefficient between the surface profile and the reflected field phase is about -0.75 when the observation plane is just above the rough surface. This simple relation between the phase of the reflected field and the surface profile is valid only near the rough surface (by elevation of the observation plane up to one wavelength above the rough surface) as is shown in Fig. 6. The phase shifts due to different elevations of the observation point above the surface have been compensated in Fig. 6. The magnitude of the reflected field cannot easily be associated with the surface profile (Fig. 7). Spatial variations of the reflected field magnitude change considerably with the elevation of the observation plane. With increase of the surface rms height σ_h, the deviations of the magnitude and the phase of the reflected field increase (Figs. 7 and 8). While spatial variations of the magnitude change with increase of σ_h, the variations of the phase still follow the surface profile.

The relationship between the surface profile and the reflected field phase explains why adding the phase term $\exp[-j\gamma_0(\kappa_0)\zeta(x)]$ into the description of the reflected field

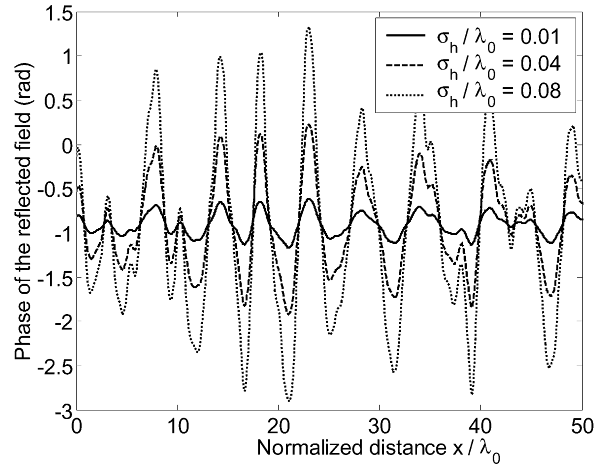

Fig. 8. Phase of the reflected field versus distance over the patch for different values of the surface rms height. The elevation of the observation point above the mean position of the rough surface equals $0.33\lambda_0$. The dielectric permittivity of the ground ε_{2r} equals 6, and the ground conductivity σ_2 equals 0.01 S/m.

(13) considerably improves performance of the perturbative methods. This relationship also provides a principal possibility to reconstruct the surface profile from the phase measurements of the reflected field near the ground. Such reconstruction will not be exact, because the correlation coefficient between the surface profile and the reflected field phase is less than 1 in absolute magnitude. However, this "qualitative" reconstruction is possible and it is much simpler than previously suggested algorithms, which require measurements of both magnitude and phase of the electric field scattered in all directions from the surface [22]. The measurement techniques for such kind of measurements are already developed for the antenna near-field measurements. The experimental proof of principal possibility to measure the scattered field phase and reconstruction the surface profile has been recently done in IRCTR [23].

The next step of the analysis is the investigation of field reflected from a statistical ensemble of surfaces. We start with analysis of distribution of magnitude and phase of the reflected field (Figs. 9 and 10). With increase of the surface rms height σ_h one can observe increase of dispersion on the distribution of magnitudes and on the distribution of phases. The latter is especially important because it causes a decrease of the mean value of the reflected field $E_{\mathrm{r,mean}}$. Figs. 9 and 10 mean that the major impact of the surface roughness (in the range $\sigma_h \leq 0.1\lambda_0$ and for the selected surface correlation function) is the phase modulation of the reflected field. Under the assumptions of this study, this modulation is proportional to the local height of the surface and thus it increases with increase of ratio σ_h/λ_0. At the same time, the magnitude of the reflected field is much less effected by the surface roughness.

Variations of the spatial length of the surface correlation function (which can be technically simulated by variations of the lower cutoff wavenumber in the surface power spectrum) cause mainly changes in the magnitude distribution of the reflected field (Figs. 11 and 12). As the rms height of the surface by these variations remain unchanged, the phase distribution remains almost constant. This results in almost constant value of the mean reflected field $E_{\mathrm{r.mean}}$.

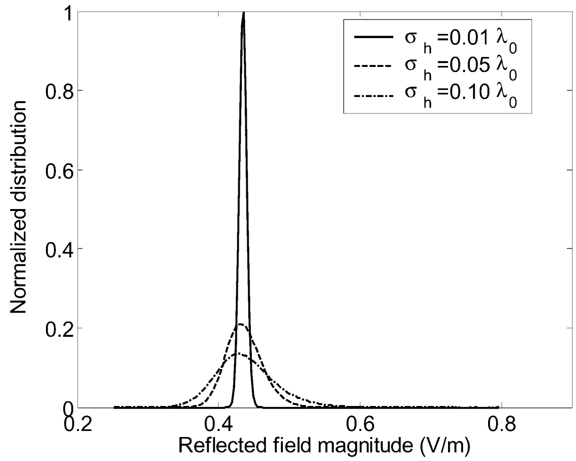

Fig. 9. Distribution of the reflected field magnitude for different values of the surface rms height. The elevation of the observation point above the mean position of the rough surface equals $0.33\lambda_0$. The dielectric permittivity of the ground ε_{2r} equals 6, and the ground conductivity σ_2 equals 0.01 S/m.

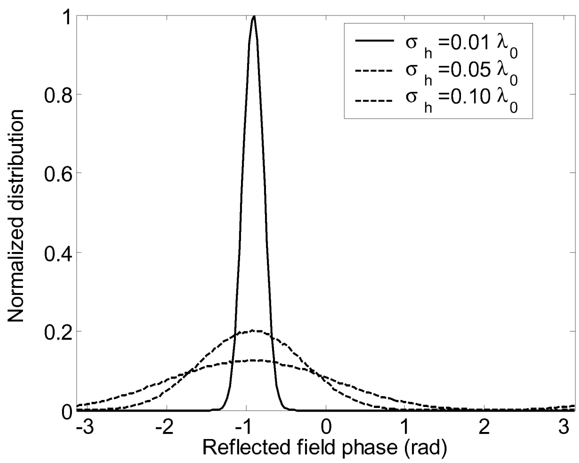

Fig. 10. Distribution of the reflected field phase for different values of the surface rms height. The elevation of the observation point above the mean position of the rough surface equals $0.33\lambda_0$. The dielectric permittivity of the ground ε_{2r} equals 6, and the ground conductivity σ_2 equals 0.01 S/m.

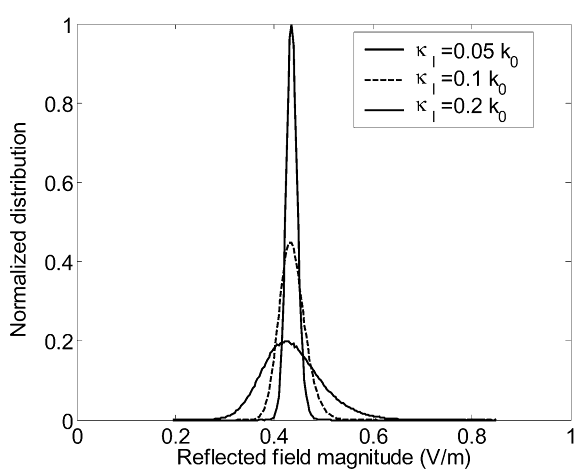

Fig. 11. Distribution of the reflected field magnitude for different values of the lower cutoff wavenumber κ_l of the surface power spectrum ($s = 3.5$, $\kappa_u = 2k_0$, $\sigma_h = 0.05\lambda_0$). The elevation of the observation point above the mean position of the rough surface equals $0.33\lambda_0$. The dielectric permittivity of the ground ε_{2r} equals 6, and the ground conductivity σ_2 equals 0.01 S/m.

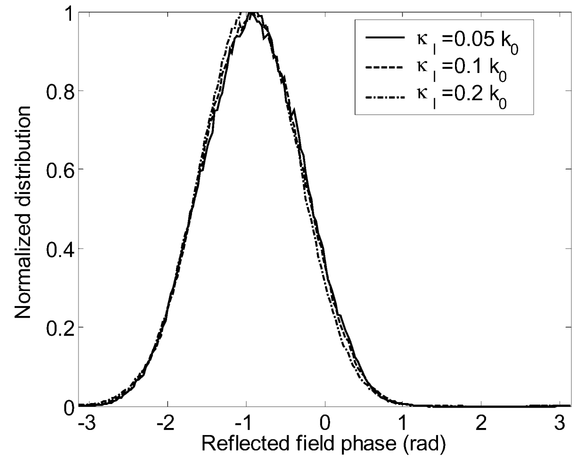

Fig. 12. Distribution of the reflected field phase for different values of the lower cutoff wavenumber κ_l of the surface power spectrum ($s = 3.5$, $\kappa_u = 2k_0$, $\sigma_h = 0.05\lambda_0$). The elevation of the observation point above the mean position of the rough surface equals $0.33\lambda_0$. The dielectric permittivity of the ground ε_{2r} equals 6, and the ground conductivity σ_2 equals 0.01 S/m.

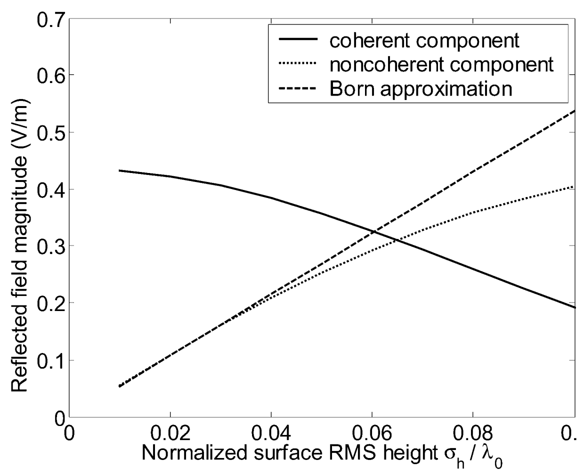

Fig. 13. Magnitude of the coherent $E_{\mathrm{r,mean}}$ and the noncoherent σ_e components of the reflected field as functions of the surface rms height σ_h. The elevation of the observation point above the mean position of the rough surface equals $0.5\lambda_0$. The dielectric permittivity of the ground ε_{2r} equals 6, and the ground conductivity σ_2 equals 0.01 S/m.

Analysis of statistical estimates of the reflected field we continue with analysis of dependency of the mean value $E_{\mathrm{r.mean}}$ and that of the standard deviation of the reflected field σ_e on rms height σ_h. These dependencies are plotted in Fig. 13. While the mean value of the reflected field decreases with an increase of σ_h, the fluctuations of the reflected field σ_e increase. The dotted line in Fig. 13 shows the dependence of σ_e predicted by the Born approximation. It can clearly be seen that already for a very small value of the surface rms height $(\sigma_h = 0.03\lambda_0)$ the "exact" value of σ_e deviates from the Born approximation. For the Gaussian surface power spectrum such a deviation has been observed for considerably larger values of rms height $(\sigma_h = 0.05\lambda_0)$ [24].

Another interesting result is that the standard deviation of the reflected field σ_e becomes larger than the mean value $E_{\mathrm{r.mean}}$ at rms height $\sigma_h \geq 0.065\lambda_0$. It means that near the rough surface, the noncoherent component of the reflected field already starts to dominate the coherent component even for reasonably

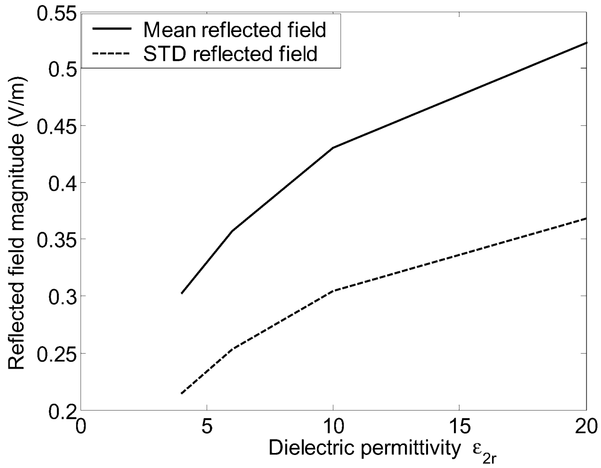

Fig. 14. Magnitude of the coherent $E_{\mathrm{r,mean}}$ and the noncoherent σ_e components of the reflected field as functions of real part of the ground dielectric permittivity. The elevation of the observation point above the mean position of the rough surface equals $0.33\lambda_0$, surface rms height equals $0.05\lambda_0$. The conductivity of the ground equals 0.01 S/m.

smooth surfaces. In other words, the magnitude of the surface clutter reaches the mean value of the reflected signal for reasonably smooth surfaces.

Both the mean value and the standard deviation of the reflected field increase with the real part of dielectric permittivity of the ground (see Fig. 14). However, while for small values of the ground dielectric permittivity (e.g., 4) and for the chosen surface power spectrum the standard deviation of the reflected field σ_e equals 1/7 of the field mean value $E_{\mathrm{r.mean}}$, for large values of the ground dielectric permittivity (e.g., 20) σ_e reaches a level of one–third for $E_{\mathrm{r.mean}}$. It means that with an increase of the real part of the dielectric permittivity, the relative value of the surface clutter increases as well.

Similar to described above dependencies of the coherent and noncoherent components of the reflected field on the surface rms height and the dielectric permittivity of the ground are predicted by far-field theories of scattering from rough surfaces (e.g., [25]). However, in these theories the noncoherent component of the reflected field is characterized not by its absolute magnitude, but by the scattering cross-section of a patch of the rough surface. So in the framework of these theories it was not possible to compare directly absolute values of the coherent and noncoherent components.

Finally the correlation function of the reflected field has been investigated (see Fig. 15). It can be seen that for very smooth surfaces ($\sigma_h = 0.01\lambda_0$) the correlation function of the reflected field repeats the correlation function of the rough surface. For larger values of the surface rms height ($\sigma_h \geq 0.05\lambda_0$) the field correlation function starts to deviate from the correlation function for the surface roughness. Taking into account the previous results, we can state that the field correlation function coincides with the correlation functions of the rough surface when the scattering is weak and the scattered field magnitude is linearly related to the Fourier spectrum of the rough surface profile (Born approximation). In practice this condition can be formulated as the condition under which the coherent component of the reflected field dominates the noncoherent component. In all

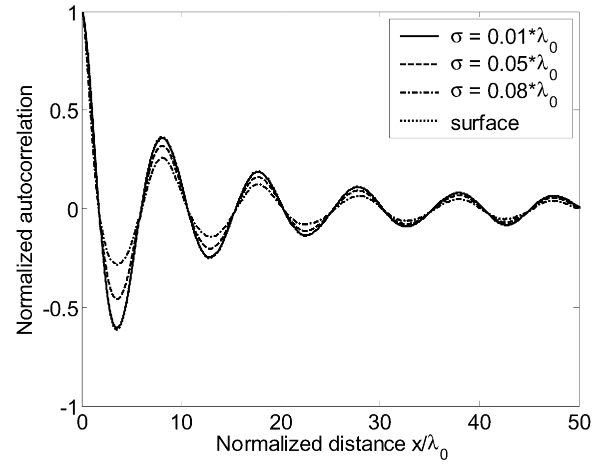

Fig. 15. Correlation function of the reflected electric field for different values of the surface rms height. The elevation of the observation point above the mean position of the rough surface equals $0.33\lambda_0$. The dielectric permittivity of the ground ε_{2r} equals 6, and the ground conductivity σ_2 equals 0.01 S/m.

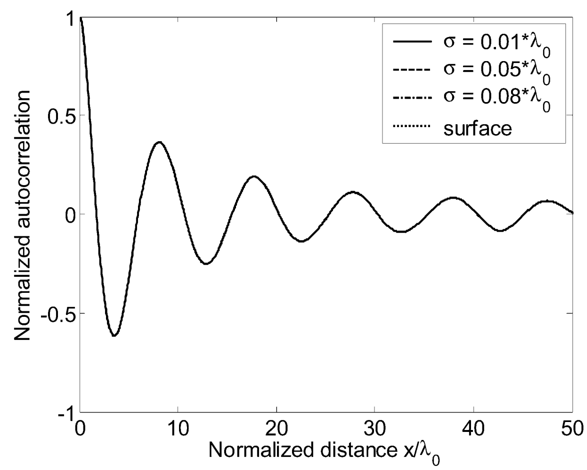

Fig. 16. Correlation function of the phase of the reflected electric field for different values of the surface rms height. The elevation of the observation point above the mean position of the rough surface equals $0.33\lambda_0$. The dielectric permittivity of the ground ε_{2r} equals 6, and the ground conductivity σ_2 equals 0.01 S/m.

simulated scenarios the correlation function of the phase of the reflected field remains the same as the correlation function of the surface roughness (Fig. 16).

VI. Conclusion

In this paper, we have analyzed the scattered field near a rough air-ground interface. The initial scattering problem has been formulated in terms of a system of two simultaneous integral equations derived by means of the extinction theorem. The Monte Carlo technique has been used to evaluate statistical properties of the scattered field. To achieve more realistic results, instead of a Gaussian spectrum of the surface roughness, we used the fractional Brownian motion model with a power-law spectrum. To speed up simulations we applied a small-slope perturbation technique to solve the system of integral equations. A benchmark solution based on the method of moments has been used to check the accuracy of the perturbation techniques for each simulation.

It has been found that the phase of the reflected field measured nearby a rough interface follows the profile of the interface, while the magnitude of the reflected field cannot be associated in a simple way with the interface profile. So the surface profile can be retrieved from the near-field interferometric measurements. Another important finding is that the phase modulation of the reflected field due to the surface roughness is the main mechanism in development of the surface clutter. The magnitude of the surface clutter exceeds the mean value of the ground reflection if the surface rms height is larger than $0.065\lambda_0$ (that is, if the real part of dielectric permittivity is about 4). With the increase of the ground dielectric permittivity, the magnitude of the surface clutter increases relatively to the averaged reflection from the ground. And finally we found that the correlation function of the reflected field coincides with the correlation function of the rough surface if the magnitude of the surface clutter is considerably less than the mean value of the ground reflection. The correlation function of the phase of the reflected field coincides with the correlation function of the surface roughness.

ACKNOWLEDGMENT

The authors would like to thank the anonymous reviewers for their comments and suggestions.

REFERENCES

[1] D. J. Daniels, *Surface-Penetrating Radar*. London: IEE, 1996.

[2] K. O'Neill, R. F. Lussky Jr., and K. D. Paulsen, "Scattering from a metallic object embedded near the randomly rough surface of a lossy dielectric," *IEEE Trans. Geosci. Remote Sens.*, vol. GE-34, pp. 367–376, Mar. 1996.

[3] P. Beckmann and A. Spizzichino, *The Scattering of Electromagnetic Waves From Rough Surfaces*. New York: Macmillan, 1963.

[4] F. G. Bass and I. M. Fuks, *Wave Scattering From Statistically Rough Surfaces*. Oxford: Pergamon, 1979.

[5] N. Garsia and E. Stoll, "Near-field effects and scattered intensities of electromagnetic waves from random rough surfaces," *J. Opt. Soc. Amer. A.*, vol. 12, pp. 2240–2243, Dec. 1985.

[6] L. Tsang, C. C. Chan, K. Pak, and H. Sangani, "Monte Carlo simulations of large -scale problems of random rough surface scattering and applications to grazing incidence with the BMIA/canonical grid method," *IEEE Trans. Antennas Propagat.*, vol. AP-43, pp. 851–859, Aug. 1995.

[7] A. G. Voronovich, "Small-slope approximation for electromagnetic wave scattering at a rough interface of two dielectric half-spaces," *Waves in Random Media*, vol. 4, pp. 337–367, 1994.

[8] V. I. Tatarskii, "The expansion of the solution of the rough-surface scattering problem in powers of quasislopes," *Waves in Random Media*, vol. 3, pp. 127–146, 1993.

[9] A. G. Yarovoy, "Small-slope iteration technique for wave scattering from a rough interface of two media," *IEEE Trans. Antennas Propagat.*, vol. AP-44, pp. 1433–1437, Nov. 1996.

[10] C. N. Vazouras, A. G. Yarovoy, M. A. Moyssidis, R. V. de Jongh, J. G. Fikioris, and L. P. Ligthart, "Application of perturbation techniques to the problem of low-frequency electromagnetic wave scattering from an air-ground interface," *Radio Sci.*, vol. 35, pp. 1049–1064, Sept.–Oct. 2000.

[11] P. C. Waterman, "Symmetry, unitarity, and geometry in electromagnetic scattering," *Phys. Rev. D*, vol. 3, no. 4, pp. 825–839, 1971.

[12] G. S. Agarwal, "Relation between waterman's extended boundary condition and the generalized extinction theorem," *Phys. Rev. D*, vol. 14, no. 4, pp. 1168–1171, 1976.

[13] A. G. Voronovich, "Small-slope approximation in wave scattering from rough surfaces," *Sov. Phys.-JETP*, vol. 62, pp. 65–70, 1985.

[14] E. Rodriguez and Y. Kim, "A unified perturbation expansion for surface scattering," *Radio Sci.*, vol. 27, no. 1, pp. 79–93, 1992.

[15] E. Rodriguez, Y. Kim, and S. L. Durden, "A numerical assessment of rough surface scattering theories: Horizontal polarization," *Radio Sci.*, vol. 27, no. 4, pp. 497–513, 1992.

[16] Y. Kim, E. Rodriguez, and S. L. Durden, "A numerical assessment of rough surface scattering theories: Vertical polarization," *Radio Sci.*, vol. 27, no. 4, pp. 515–527, 1992.

[17] R. M. Axline and A. K. Fung, "Numerical computation of scattering from a perfectly conducting random surface," *IEEE Trans. Antennas Propagat.*, vol. AP-26, pp. 482–488, May 1978.

[18] A. K. Fung and M. F. Chen, "Numerical simulation of scattering from simple and composite random surfaces," *J. Opt. Soc. Amer. A*, vol. 2, pp. 2274–2284, Dec. 1985.

[19] E. I. Thorsos, "The validity of the Kirchhoff approximation for rough surface scattering using a gaussian roughness spectrum," *J. Acoust. Soc. Amer.*, vol. 83, pp. 78–92, Jan. 1988.

[20] G. Franceschetti, A. Iodice, M. Migliaccio, and D. Riccio, "Scattering from a natural surface described by the fractional brownian motion model: Small perturbation method," in *Proc. IGARSS'99*, vol. 5, pp. 2416–2419.

[21] F. Mattia, T. L. Toan, M. Davidson, and M. Borgeaud, "On the scattering from natural rough surfaces," in *Proc. IGARSS'99*, vol. 5, pp. 2413–2415.

[22] R. J. Wombell and J. A. DeSanto, "Reconstruction of rough-surface profiles with the kirchhoff approximation," *J. Opt. Soc. Amer. A*, vol. 8, no. 12, pp. 1892–1897, Dec. 1991.

[23] B. Sai and L. P. Ligthart, "Characterization of local 3D rough surfaces using UWB near-range phase-based GPR signatures from wide-beamwidth antennas," in *Proc. IGARSS'02*, vol. 6, pp. 3582–3584.

[24] M. F. Chen and A. K. Fung, "A numerical study of the regions of validity of the kirchhoff and small-perturbation rough surface scattering models," *Radio Sci.*, vol. 23, pp. 163–170, Mar.–Apr. 1988.

[25] N. P. Zhuk and A. G. Yarovoi, "Electromagnetic wave reflection from rough interface," *Opt. Spectrosc.(USSR)*, vol. 67, no. 5, pp. 661–664, Nov. 1989.

Alexander G. Yarovoy (M'96) received the Diploma with honors in radiophysics and electronics from the Kharkov State University, Ukraine, in 1984. He received the Candidate Physics and Math. Science and Dr. Physics and Math. Science degrees in radiophysics in 1987 and 1994, respectively.

In 1987, he joined the Department of Radiophysics, Kharkov State University, as a Researcher and became a Professor there in 1997. From September 1994 through 1996, he was with Technical University of Ilmenau, Germany, as a Visiting Researcher. Since 1999, he has been with the International Research Centre for Telecommunications-Transmission and Radar (IRCTR), Delft University of Technology, The Netherlands, where he coordinates all GPR-related projects. His main research interests are in ultrawideband electromagnetics, wave scattering from statistically rough surfaces and penetrable obstacles, and computational methods in electromagnetics.

Prof. Yarovoy is the recipient of a 1996 International Scientific Radio Union (URSI) "Young Scientists Award" and the co-recipient of the European Microwave Week Radar Award in 2001 for the paper that best advances the state-of-the-art in radar technology.

Christos N. Vazouras was born in Pharsala, Greece, in 1966. He received the Dipl.Eng. and the Ph.D. degrees in 1990 and 1995, respectively, from the Department of Electrical and Computer Engineering of the National Technical University of Athens, Greece.

He has worked in the private sector on project management and MIS software development. Since 1997, he has been a Special Scientist with the Hellenic Naval Academy. His research interests include electromagnetic scattering, microwave communication systems design, wave interaction with anisotropic media, and biomedical engineering.

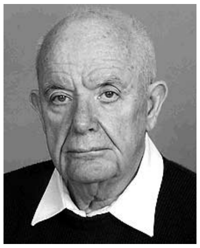

John G. Fikioris was born in Sparti, Greece, on April 9, 1931. He received the Diploma of E.E. and M.E. from the National Technical University of Athens, Greece, in 1955, the M.S.E.E. degree from Rensselaer Polytechnic Institute, Troy, NY, in 1958, and the M.A. and Ph.D. degrees in applied physics from Harvard University, Cambridge, MA, in 1963.

From 1962 until early 1966, he was a Research Scientist with the RAD division of Avco Corporation, Wilmington, MA. From January 1966 to June 1972, he was a Professor of electrical engineering with the University of Toledo, OH. In May 1972, he was elected Professor of Wireless and Long Distance Communications at the National Technical University of Athens (NTUA). He held this position until his retirement in September 1998 as Professor Emeritus of NTUA. His main fields of interest include antennas and wave propagation, guiding phenomena, wave optics, diffraction and scattering, acoustic and electromagnetic field evaluations in the source region, singular integral equations, and applied mathematics.

Dr. Fikioris is a Member of Sigma Xi. He served as Chairman of the International Scientific Radio Union (URSI) Member Committee for Greece from 1981 to 1998.

Leo P. Ligthart (M'94–SM'95–F'02) was born in Rotterdam, The Netherlands, on September 15, 1946. He received the Engineer's degree (*cum laude*) and the Doctor of Technology degree from Delft University of Technology, The Netherlands, in 1969 and 1985, respectively, and the Doctorates (*honoris causa*) from Moscow State Technical University of Civil Aviation, Moscow, U.S.S.R., in 1999 and Tomsk State University of Control Systems and Radioelectronics in 2001.

Since 1992, he has held the Chair of Microwave Transmission, Radar and Remote Sensing, Department of Information Technology and Systems, Delft University of Technology. In 1994, he became Director of the International Research Center for Telecommunications-Transmission and Radar. His principal areas of specialization include antennas and propagation and radar and remote sensing. He has also been active in satellite, mobile, and radio communications.